Molecular structure of the NQTrp inhibitor with the Alzheimer Aβ1–28 monomer

ARTICLE *in* EUROPEAN JOURNAL OF MEDICINAL CHEMISTRY · JULY 2014

Impact Factor: 3.45 · DOI: 10.1016/j.ejmech.2014.07.002 · Source: PubMed

European Journal of Medicinal Chemistry 91 (2015) 43–50

Contents lists available at ScienceDirect

European Journal of Medicinal Chemistry

journal homepage: http://www.elsevier.com/locate/ejmech

Original article

Molecular structure of the NQTrp inhibitor with the Alzheimer Aβ1-28 monomer

Bogdan Tarus [a], Phuong H. Nguyen [a], Olivia Berthoumieu [b, c], Peter Faller [b, c], Andrew J. Doig [d], Philippe Derreumaux [a, e, *]

[a] Laboratoire de Biochimie Théorique, UPR 9080 CNRS, Université Paris Diderot, Sorbonne Paris Cité, IBPC, 13 Rue Pierre et Marie Curie, 75005 Paris, France
[b] CNRS, LCC (Laboratoire de Chimie de Coordination), 205 Route de Narbonne, BP 44099, F-31077 Toulouse Cedex 4, France
[c] Université de Toulouse, UPS, INPT, F-31077 Toulouse Cedex 4, France
[d] Manchester Institute of Biotechnology, Faculty of Life Sciences, The University of Manchester, 131 Princess Street, Manchester M1 7DN, UK
[e] Institut Universitaire de France, IUF, 103 Boulevard Saint-Michel, 75005 Paris, France

ARTICLE INFO

Article history:
Received 29 April 2014
Received in revised form
19 June 2014
Accepted 1 July 2014
Available online 1 July 2014

Keywords:
Amyloid simulations
Alzheimer
Aβ monomer
Drug
Intrinsic disorder
All-atom replica exchange molecular dynamics

ABSTRACT

The self-assembly of the amyloid-β (Aβ) peptide of various amino acid lengths into senile plaques is one hallmark of Alzheimer's disease pathology. In the past decade, many small molecules, including NQTrp, have been identified to reduce aggregation and toxicity. However, due to the heterogeneity of the conformational ensemble of Aβ with drugs, we lack detailed structures of the transient complexes. Following our previous simulation of the monomer of Aβ1-28, here we characterize the equilibrium ensemble of the Aβ1-28 monomer with NQTrp by means of extensive atomistic replica exchange molecular dynamics simulations using a force field known to fold diverse proteins correctly. While the secondary structure content and the intrinsic disorder of the whole peptides are very similar and the lifetimes of the salt-bridges remain constant, the population of β-hairpin is reduced by a factor of 1.5 and the population of α-helix in the region 17–24 is increased by a factor of two upon NQTrp binding. These two factors, which impact the free energy barrier for nucleation, provide a first explanation for the reported reduced Aβ1-40/1-42 aggregation kinetics in the presence of NQTrp. Backbone and side-chain interactions of Aβ with NQTrp may also inhibit Aβ–Aβ contacts. The fraction of free Aβ1-28 monomer is, however, on the order of 20–25% at 17.5 mM, and this shows that the affinity of NQTrp is low and hence its inhibitory activity is not very strong. This inhibitor can be improved to reduce the formation of dimer, a critical step in aggregation and toxicity.

1. Introduction

One of the hallmarks of Alzheimer's disease (AD) is the aggregation of β-amyloid peptides of 40 (Aβ1-40) and 42 (Aβ1-42) residues into insoluble amyloid plaques found in the brain [1]. The human Aβ1-42 sequence is DAEFRHDSGYEVHHQ KLVFFAEDVGSN KGAIIGLMVGGVVIA with a charged N-terminus (Asp1–Lys16) and two hydrophobic patches Leu17–Ala21 (central hydrophobic core, CHC) and Ala30–Ala42 (C-terminus) separated by a hydrophilic patch Glu22–Gly29. There is increasing evidence that all species from dimers to fibrils are pathogenic agents [2,3] and therefore blocking the monomer–dimer transition has been a long-standing goal in the treatment of AD.

In the past decade, many large biomolecules have been identified to bind strongly to the monomeric state of Aβ1-42/1-40 as well as Aβ dimers, trimers and tetramers preventing further aggregation. These include the *Escherichia coli* maltose binding protein [4] and a Green fluorescent protein variant with the first and sixth strands substituted by amino acids corresponding to the residues 14–23 of Aβ [5]. Hoyer et al. also reported that the phage-display selected affibody ZAβ3 dimer binds to Aβ1-40 monomer with nanomolar affinity and inhibits Aβ1-40 fibrillation at stoichiometric concentrations [6]. Breaching the blood–brain barrier remains an obstacle, however, for delivery of large therapeutics including proteins and antibodies [7].

Owing to their physical–chemistry properties, small molecules are more amenable to blood–brain delivery, but have lower affinities. These include: (1) peptide ligands, such as SEN304 with D-

* Corresponding author. Laboratoire de Biochimie Théorique, UPR 9080 CNRS, Université Paris Diderot, Sorbonne Paris Cité, IBPC, 13 Rue Pierre et Marie Curie, 75005 Paris, France.
E-mail address: philippe.derreumaux@ibpc.fr (P. Derreumaux).

http://dx.doi.org/10.1016/j.ejmech.2014.07.002
0223-5234/

and N-methylated amino acids [8] and a peptide [9] with N-methylated amino acids which, by recognizing the amino acids 16–20 and 32–37 of Aβ, reduces both aggregation and toxicity, (2) compounds such as orcein, which accelerates fibril formation and thus reduces the lifetimes of the transient toxic species [10], (3) molecules occurring naturally in human brain tissues at relatively high concentrations (1–20 mM), such as β-alanyl-L-histidine dipeptide or carnosine, which inhibits Aβ1-42 aggregation *in vitro* [11], and (4) synthetic compounds either reducing the rate of fibril fragmentation and in turn toxicity [12], or reported to reduce Aβ oligomers' toxicity and recover the phenotype in a transgenic AD drosophila model, such as 1,4-naphthoquinon-2-yl-L-tryptophan NQTrp [13].

The structures of Aβ1-40/1-42 monomers and Aβ1-40/1-42 oligomers with small inhibitors are currently unknown due to the transient and heterogeneous ensemble of conformations. Using a shorter fragment and a 0.25 M ratio of NQTrp to Aβ, Segal et al. proposed a 3D structure of NQTrp bound to the Aβ12-28 monomer based on NMR resonance shifts, 177 NOE intramolecular interactions with only four interactions involving residues $i, j > i + 5$, and free of any NOE between the peptide and the inhibitor [13]. The binding mechanism of NQTrp to Aβ12-28 studied by molecular dynamics (MD) simulations with an implicit solvent model and an all-atom representation for the peptide and NQTrp revealed three dominant binding sites between NQTrp and the Aβ18-21 region [13]. MD simulations using the implicit FACTS solvent model and the united-atom CHARMM19 force field of the Aβ12-28 monomer with one NQTrp reported there are no predominant binding modes, although NQTrp preferentially interacts with the residues spanning His13–Phe20 and the side-chains of Phe19 and Phe20 constituting the site of highest interaction probability [14]. A multi-scale approach consisting of replica exchange molecular dynamics (REMD [15]) based on the coarse-grained OPEP force field [16], followed by all-atom docking calculations revealed NQTrp is the best binder to Aβ17-42 trimeric structures among five small-molecule drugs, including EGCG and resveratol [17]. These simulations also showed that NQTrp has multiple binding modes with different affinities, although it interacts preferentially with the CHC region (residues 17–21). The binding to the CHC region was supported by all-atom REMD simulations of the Aβ1-42 dimer with two NQTrp molecules, which showed that NQTrp can also interact with the hydrophobic residues Leu34 and Met35 and the hydrophilic residues Arg5, Tyr10, Lys16, Asp7 and Arg28 [18]. These simulations also emphasized that there are many binding sites with small percentage occupancies and the average contact surface for each site is much smaller than those typically observed in the PDB protein–drug complexes.

The goal of this study is to provide, by means of extensive atomistic REMD simulations using a force field known to fold diverse proteins correctly, a clear mechanistic picture of the interaction of NQTrp with the Aβ1-28 monomer in an 'experimental-like' buffer. The Aβ1-28 monomer, rather than the Aβ1-40/1-42 monomer, was chosen for the following reasons: Aβ1-28 forms fibrils with in register parallel β-sheets, as in the Aβ1-40 and Aβ1-42 fibrils [19], and the γ-secretase generates mostly peptides from Aβ1-36 to Aβ1-43, but Aβ1-30 and Aβ1-26 peptides were reported by mass spectrometry (MS) analyses of human AD brains [20]. Electrospray ionization MS (EI-MS) showed that low molecular weight compounds bind similarly to Aβ1-42, Aβ1-40 and Aβ1-28 peptides [21]. We recently characterized the free energy landscape of the Aβ1-28 monomer by means of atomistic REMD simulations, and found that the predicted equilibrium ensemble at 315 K is fully consistent with circular dichroism, ion mobility MS and diffusion NMR data and revealed the high intrinsic disorder of the Aβ1-28 monomer [22]. Finally, as Aβ1-28 is much less prone to aggregation than the Aβ1-40 and Aβ1-42 peptides, our predictions can be more easily tested experimentally. For simplicity, in what follows the Aβ1-28 peptide will be designated as Aβ, unless specified.

2. Materials and methods

2.1. Simulations details

The initial coordinates of Aβ were taken from the NMR structure of Aβ1-40 in a membrane-like environment with two α-helices spanning residues 8–25 and 28–39 [23]. This state was selected because it was used as the starting point of the REMD simulation of Aβ1-28 alone [22]. The monomer with unblocked termini was then placed in a box of explicit water and subjected to MD simulation for 5 ns at 500 K. The final random coil structure was selected and NQTrp, modeled by an all-atom representation, was oriented randomly and separated from the side-chain extremities of Phe19 and Phe20 by two solvation shells. Subsequently, the complex was placed in a truncated octahedron box with periodic conditions and a volume of 94.8 nm^3 with 2932 TIP3P molecules. Phosphate ions $H_2PO_4^-$ and HPO_4^{2-} at a concentration of 20 mM and a molar ratio of 1:1 were added to mimic the experimental conditions often used for amyloid formation. The pH was set to 7 with the N-terminus treated as NH_3^+ and the C-terminus as CO_2^-, Arg and Lys positively charged (NH_3^+), Glu and Asp negatively charged (CO_2^-), and the His residues neutral with a hydrogen on the epsilon nitrogen. Finally, the system was neutralized by adding 7 K^+ cations, resulting in 9296 atoms. Note in the experimental studies we performed we did not add sodium but potassium (in preparation).

The GROMACS program [24] (version:4.5.5) was used to perform the simulations. The bond lengths with hydrogen atoms were fixed with the SHAKE algorithm [25] and the equations of motion were integrated with a time step of 2 fs using the velocity Verlet integrator. The electrostatic interactions were calculated using the particle mesh Ewald method and a cutoff of 1.1 nm [26]. A cutoff of 1.2 nm was used for the Van der Waals interactions. The nonbonded pair lists were updated every 10 fs. Temperatures were controlled by the velocity-rescaling thermostat, developed by Bussi–Donadio–Parinello and found to sample the canonical ensemble [27]. Following the simulation of Aβ alone [22], we used the CHARMM22* force field rather than the GROMOS and OPLS force fields [28] because it allows folding diverse proteins into their NMR structures [29]. This force field has, however, some limitations for reproducing melting temperatures [29] and vibrational frequency modes with high accuracy [30,31] .

2.2. NQTrp parametrization

The Marvin program [32] was used to build the 3D chemical structure of levo-NQTrp and the buffer ions that were subsequently saved as PDB format. Fig. 1 depicts the chemical structure of NQTrp with the labeling of the heavy atoms. The Maestro package [33] was then employed to convert the coordinates from PDB to mol2 format

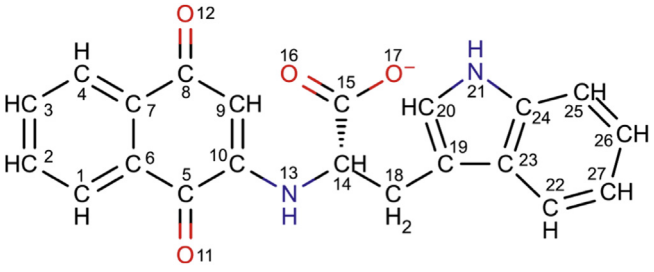

Fig. 1. The all-atom structure of NQTrp with the heavy atoms labeled.

and the coordinates were uploaded on the ParamChem interface [34] to obtain CHARMM topologies and parameters for small molecules using the 0.9.6 beta program [35] and the CHARMM General Force Field version 2b7 [36]. Although our NQTrp parameters do not match exactly those used in previous simulations of Aβ with NQTrp [14,18], the partial charges of some NQTrp atoms changing by 0.05 electronic units, the parameter sets are comparable.

2.3. Simulation time and analysis

REMD was carried out with 48 replicas, varying from 290 K to 466 K, using the temperature method developed by Patriksson and van der Spoel [37]. Exchanges between neighboring replicas were attempted every 2 ps, leading to an average acceptance ratio of 25%. Each replica ran for 205 ns, and we excluded the first 50 ns for analysis. The secondary structures were calculated using STRIDE [38]. The eight STRIDE structures were grouped into four structures: β-strand = extended + bridge, α-helix = α-helix + 3_{10}-helix, turn = turn + bend, and coil = coil + P_{II}-helix. Note that the percentage of 3_{10}- and P_{II}-helices is very low in the present simulation. A Cα–Cα contact was defined if the distance is less than 5 Å and a side-chain–side-chain contact was considered formed if the distance between their centers of mass is <6.5 Å. A hydrogen bond (H-bond) was considered formed when the acceptor–donor distance is not more than 3.5 Å, and the acceptor–donor–hydrogen angle is not more than 30°. A salt-bridge (SB) between two charged side-chains was considered formed if the distance between two specific atoms remains within 4.6 Å [39]. We also defined a β-hairpin if there are at least two backbone H-bonds formed between consecutive β-strands, and at least three consecutive residues belonging to the β Ramachandran region in each strand [22].

The conformations of Aβ in the presence of NQTrp were also analyzed using the root-mean square deviation (RMSD) and principal component analysis (PCA). The Cα RMSD clustering was performed using the linkage algorithm with a cutoff of 0.25 nm. Following our previous work, we used PCA using the inverse distances between Cα atoms, rather the dihedral angles, to describe the collective motions [22]. To facilitate a direct comparison between Aβ alone and Aβ in the presence of NQTrp, we used the same eigenvectors by combining the two trajectories and performed PCA analysis by projecting the trajectory of Aβ/NQTrp on the obtained eigenvectors. In our systems, the first three principal components account for up to 60% of the fluctuations. To identify geometric clusters in this subspace, we carried out clustering analysis as described in Ref. [22]. Statistical errors were estimated by block (time interval) averaging.

3. Results

3.1. REMD convergence

The convergence of the simulation for Aβ in the presence of NQTrp was assessed at 315 K, near the physiological temperature, by using five criteria calculated over two or three time intervals (50–150 and 50–205 ns for the first four criteria, and 50–102, 102–154, and 154–205 ns for the last one). These criteria are the distribution of the radius of gyration (R_g), the distribution of the Cα end-to-end distances (d_{ee}), the distribution of the total number of contacts between the Cα atoms (N_c), the average solvent accessible surface area (SASA) of each amino acid, and the average turn probability of each amino acid. We clearly see in Fig. 2 that the five metrics reach equilibrium values at 315 K after 205 ns per replica. Comparing the two systems, Aβ with and without NQTrp, the R_g

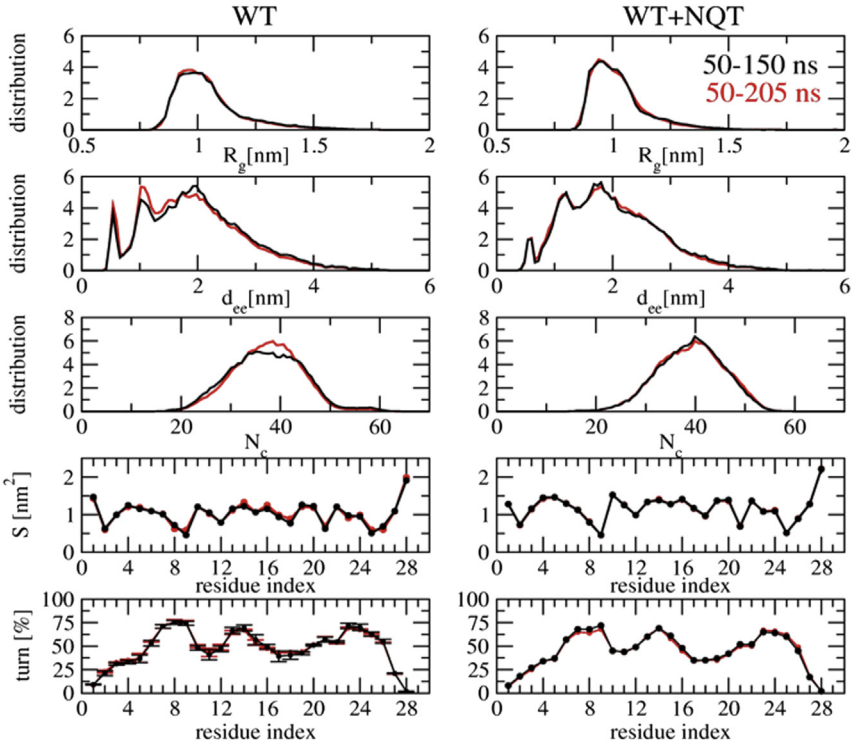

Fig. 2. Convergence of REMD simulations at 315 K for the Aβ alone (left) and in the presence of NQTrp (right) assessed using five metrics. Distributions of the radius of gyration (R_g), Cα end-to-end distances (d_{ee}), total number of contacts between Cα atoms (N_c), and the solvent accessible surface area (S) of each residue. These distributions were calculated over two time intervals, 50–150 ns (black) and (50–205) ns (red). The bottom panel depicts the turn propensity of each amino acid, with statistical errors calculated using a block average technique over three time intervals, 50–102, 102–154, and 154–205 ns. All these metrics calculated over different time intervals indicate the convergence of the REMD simulations. (For interpretation of the references to color in this figure legend, the reader is referred to the web version of this article.)

distributions are identical and the distributions of the end-to-end distances are also very similar, even if the d_{ee} population at short distances decreases from 4% to 2% upon NQTrp binding. The overall values of R_g and d_{ee} indicate flexible, unfolded conformations of Aβ in both systems. The distributions of N_c contacts, and the SASA and turn profiles along the sequence do not show any significant variation in the global properties of Aβ upon NQTrp binding.

3.2. Secondary structures and salt-bridges

The interaction with NQTrp does not change the secondary structure of the peptide at 315 K. The populations of turn and coil dominate, 48.3 ± 2.5% and 34.6 ± 2.7% in Aβ alone vs. 44.8 ± 2.6% and 34.3 ± 2.6% in the complex. The β-strand content remains constant at 10.0 ± 2%, and the α-helix content increases from 7.2 ± 1.4 to 11.1 ± 2.0% upon NQTrp binding. The presence of the NQTrp does not change much the coil and turn contents along the sequence (Fig. 3, bottom left panel). In contrast, we see variations in the β-strand probabilities at specific positions (Fig. 3, upper left panel). While the amino acids spanning 3–5, 10–12, and 16–20 have mean β-strand values of 19.7, 23.5 and 18.4% in Aβ alone, they have mean values of 24.0, 18.6 and 19.4% in Aβ within the complex. The presence of NQTrp also increases the α-helix content of residues 7–11 (from 7 to 14%), residues 17–21 (10 to 17%), and residues 22–25 (12 to 21%). Note that the statistical errors in these β-strand and α-helix values do not exceed ±1.6%.

Most of the salt-bridges between Aβ charged residues have lifetimes <10% in both systems at 315 K (Fig. 4). The salt-bridges between Glu3 and Arg5, Arg5 and Asp7, and Asp23 and Arg28 have populations of 16, 16 and 12%, respectively, in Aβ alone, while these values shift to 17, 10 and 10% in the presence of NQTrp. With NQTrp, the population of the salt-bridge between Asp7 and Lys16 decreases from 6 to 3%, favoring an increase of the lifetimes of the salt-bridges between Lys16 and Asp23 and between Glu22 and Lys28 from 3 to 8% and 6 to 9%, respectively.

Overall analysis of the five metrics, the secondary structure composition and the lifetimes of salt-bridges using different time windows demonstrates that the REMD results do not depend on the initial structure.

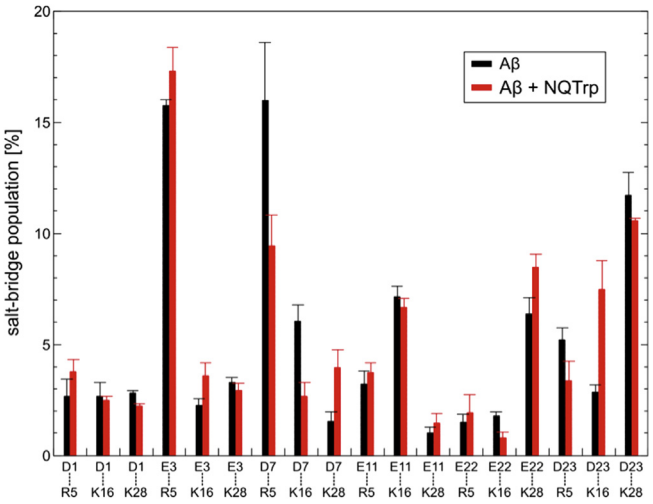

Fig. 4. Probabilities of salt-bridges formation between all charged residues at 315 K. Aβ alone (black bars) and in the presence of NQTrp (red bar) using the time interval of 50–205 ns. Statistical errors are calculated using a block average technique over three time intervals, 50–102, 102–154, and 154–205 ns. (For interpretation of the references to color in this figure legend, the reader is referred to the web version of this article.)

3.3. Impact of NQTrp on the conformational ensemble of Aβ

Fig. 5 displays the result of the RMSD clustering of the conformations of Aβ in isolation (black curve) and in the presence of the NQTrp (red curve) using a cutoff of 0.25 nm at 315 K. The conformations of Aβ in isolation can be described by 2507 clusters, with 2.3% of the structures in the most populated cluster. Adding NQTrp to the Aβ drops the number of clusters to 1857 and increases the population of the dominant state to 4.0%. Overall, NQTrp induces an observable difference in the population of the first four states (13% vs. 8%, Fig. 5), but does not prevent the intrinsic disorder of the Aβ peptide.

To get insights into the equilibrium ensemble at 315 K, Table 1 describes the structural characteristics of the dominant clusters of Aβ in the complex on the subspace spanned by the first three

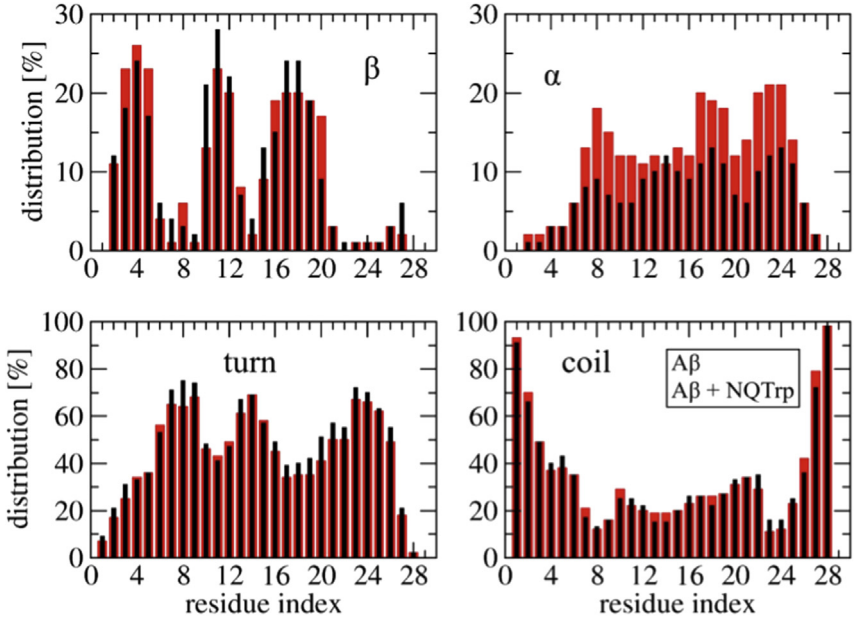

Fig. 3. Secondary structure propensities along the amino acid sequence of Aβ alone (black bars) and in the presence of NQTrp (red bar) at 315 K using the time interval of 50–205 ns. (For interpretation of the references to color in this figure legend, the reader is referred to the web version of this article.)

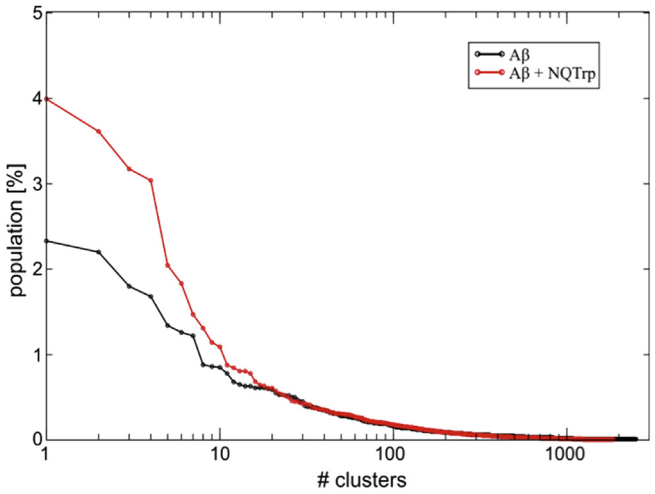

Fig. 5. Equilibrium population of all clusters for Aβ alone (black) and Aβ with NQTrp (red) at 315 K. A semi-logarithmic representation is used for clarity. The clustering was performed over the time interval 50–205 ns. (For interpretation of the references to color in this figure legend, the reader is referred to the web version of this article.)

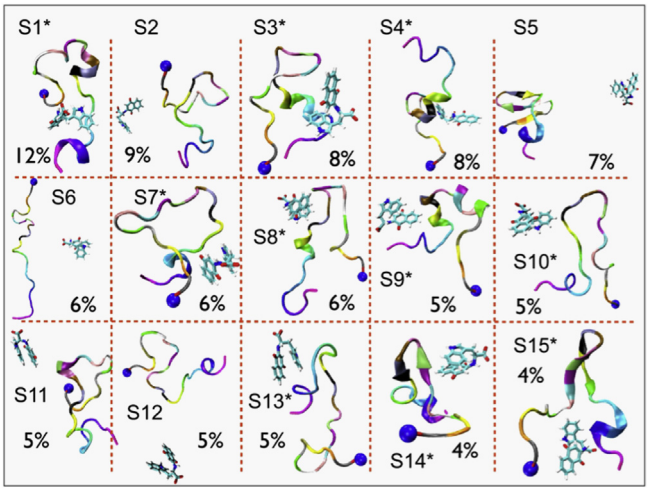

Fig. 6. Representative structures of Aβ in presence of NQTrp corresponding to the 15 clusters built using the first three principal components, V1, V2, and V3. The blue sphere indicates the N-terminus. The asterisks show conformations where the peptide and drug are in contact. The clustering was performed on the time interval 50–205 ns at 315 K. (For interpretation of the references to color in this figure legend, the reader is referred to the web version of this article.)

principal components using the full ensemble of 1857 conformations. The analysis for Aβ alone is reported elsewhere [22]. Representative structures of the first 15 PCA-based clusters of Aβ in the complex, designated as S1–S15, are drawn in Fig. 6. The representative structure refers to the center of a cluster. Table 1 presents for each cluster, its probability and average secondary structure composition, the average population of hydrogen bonds between two β-strands (P_{HB}), the average population of β-hairpins (P_{2s}), and the average Cα end-to-end distance (d_{ee}). Table 1 also provides the RMSD deviations of the centers of all clusters with respect to the center of the first cluster and the average RMSD deviations of all members of each cluster with respect to its center. The average values were obtained by using all conformations belonging to each cluster.

Looking at the first ten clusters of Aβ alone and in the complex, representing 67% and 72% of all conformations, respectively, the fractions of turn and coil are similar. In isolated Aβ, the β-strand varies from 4 to 24%, the α-helix from 4 to 11%, and P_{2s} from 5 to 23% [22], while the corresponding values in the complex vary from 3 to 16%, 8 to 16%, and 1.5 to 5.5%. Direct contacts between NQTrp and Aβ thus increase the α-helix content (see S1, S3, S4, S7, S8, S9 and S14 in Fig. 6 with probabilities varying from 12 to 4%), and reduce substantially the formation of β-hairpins (see S14 and S15 with probabilities of 4%). For comparison, in Aβ alone, only 3% of all conformations form β-hairpins, and 20% of all conformations form α-helix [22]. It has to be noted that the two rings of NQTrp do not always interact with the peptide at the same time (see S4 in Fig. 6). The probability that one ring and two rings of NQTrp are in contact with the peptide is 42 and 32%, respectively.

A second interesting feature of the free energy landscape is that among the first 15 clusters, the five clusters S2, S5, S6, S11 and S12 do not form any contacts between the peptide and NQTrp. These four states are characterized by turn + coil percentages varying from 82 to 78% and end-to-end distances of 2.0, 1.5, 3.3 and 1.9 Å. There is no structural similarity between these states. S5 forms a three-stranded β-sheet, S11 and S12 are random coil, and S6 is a rather fully extended state, very similar to the S6 state observed in the free energy landscape of Aβ alone [22]. Overall using all

Table 1
PCA analysis of the dominant conformations of Aβ with NQTrp at 315 K. For each cluster, we give its population and the average secondary structure composition (in %), the average population in % of hydrogen bonds between two β-strands (P_{HB}) and of β-hairpins (P_{2s}), the average Cα end-to-end distance (d_{ee}, in Å), the RMSD value (in nm) of all cluster members with respect to the center of the cluster ($RMSD_1$), and the RMSD (in nm) of the centers of all clusters with respect to the center of the first cluster ($RMSD_2$). The high values of $RMSD_1$ emphasize the limitation of one collective variable to describe the energy landscape.

	Cluster	P	β-strand	α-helix	Turn	Coil	P_{HB}	P_{2s}	d_{ee}	$RMSD_1$	$RMSD_2$
Aβ + NQTrp	1	12.24	16	8	37	39	3.74	2.55	1.58	0.58	0.00
	2	9.06	11	10	46	32	3.53	2.38	2.05	0.58	0.78
	3	7.61	14	9	40	37	3.32	1.90	1.50	0.59	0.54
	4	7.55	5	11	50	35	7.74	5.45	2.56	0.69	0.74
	5	6.75	6	16	45	33	5.66	4.36	1.54	0.64	0.71
	6	6.43	3	10	48	39	2.69	1.62	3.35	0.73	1.05
	7	6.41	4	16	43	36	1.59	1.45	1.46	0.60	0.71
	8	5.98	8	10	45	37	4.45	3.88	2.38	0.64	0.78
	9	5.44	3	14	49	34	2.54	2.25	1.91	0.64	0.79
	10	5.39	15	13	44	28	9.02	7.80	1.86	0.62	0.82
	11	5.17	15	8	47	30	1.02	0.90	1.54	0.62	0.62
	12	5.03	8	12	48	32	1.41	1.33	2.26	0.64	0.71
	13	4.97	14	10	44	32	1.40	1.40	1.56	0.65	0.74
	14	4.56	4	15	47	35	4.05	3.74	1.70	0.60	0.61
	15	3.81	13	6	47	33	7.69	4.64	2.31	0.59	0.81
	16	3.61	19	7	46	28	12.72	7.22	1.44	0.56	0.76

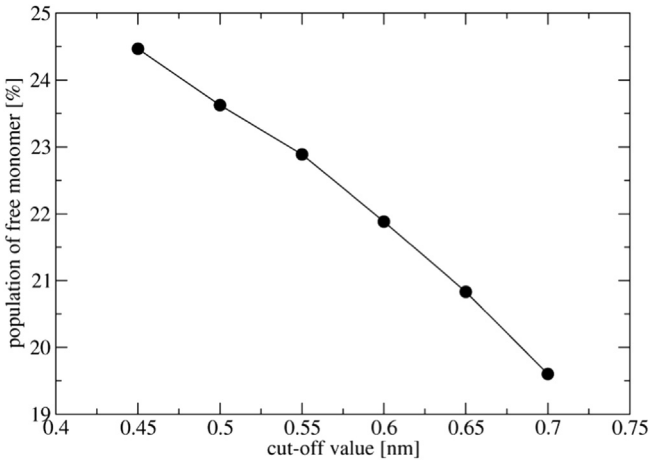

Fig. 7. Population of free Aβ monomer at 315 K calculated in the Aβ/NQTrp system as a function of the smallest distance between any heavy atoms of the two molecules.

conformations, the peptide is free of any contact with NQTrp in 19.5–24.5% of the simulation time, as reported in Fig. 7.

Fig. 8 display the contacts between the heavy atoms of the NQTrp and the atoms of either the Aβ side-chains (left panel) or the backbone (right panel). We can identify 13 spots between NQTrp and the side-chains of hydrophilic residues Asp1, Arg5, Asp7, Tyr10, His13, Gln15, Lys16 and Glu22, and hydrophobic residues of the CHC region with contact probabilities varying between 1.5 and 3.0%, but all other residues contribute as well with lower probabilities, except the two C-terminal residues. We can also identify 15 spots between NQTrp and the main chain atoms of Phe4, Arg5, His6, Gly9, Tyr10, His12, His13, Lys16, Glu22, Arg28 and the CHC region with contact probabilities varying between 2.0 and 5.0%.

Finally, since $H_2PO_4^-$ and HPO_4^{2-} were added to mimic the experimental conditions, and unlike commonly used chloride ions, phosphate ions may have different orientation/hydrogen bonding and Van der Waals interactions with the peptide, we analyzed their contact probabilities with the backbone and side-chains. We find that HPO_4^{2-} interacts with the backbone of Asp1 (lifetime of 11%) and to a lesser extent with the side-chains of Asp1, Arg5, Lys16 and Asp28 (lifetimes of 3.5–5%). $H_2PO_4^-$ interacts with the same pattern of residues, but with much lower lifetimes: 1.2–2% with the backbone of Asp1, and 0.7–1.0% with the side-chains of Asp1, Arg5, Lys16 and Asp28.

4. Discussion and conclusions

It has been shown experimentally that NQTrp reduces the aggregation propensity and toxicity level of the Aβ1-40 and Aβ1-42 peptides [13]. Previous united-atom MD simulations in implicit solvent between NQTrp and shorted Aβ fragments, such as Aβ14-20, Aβ16-22, Aβ16-24 and Aβ12-28 [13,14,40] reported that the most favorable contacts span the residues 13–20 [14,40]. Recently, extensive atomistic REMD simulations in explicit solvent of the Aβ1-42 dimer with two NQTrp identified that the most favorable binding residues are Arg5, Asp7, Tyr10, His13, Lys16, Val18, Phe19/Phe20, and Leu34/Met35 [18].

Our simulations on Aβ1-28 monomer revealed that NQTrp forms transient interactions with all amino acids, although binding sites of higher probabilities are found at residues Asp1, Arg5, Asp7, Tyr10, His12, His13, Lys16, Glu22, Ser26, Arg28, and the hydrophobic patch spanning residues Leu17–Ala21. This binding picture is therefore very different with the MD results of Aβ12-28 with NQTrp [14,40]. This indicates that NQTrp interactions with Aβ peptides are very sensitive to the Aβ peptide length, and notably the presence of residues spanning 1–11. The impact of the N-terminus is also seen in the reduction of the lifetimes of the salt-bridges involving Arg5 which in turn increases the lifetime of the salt-bridge between Lys16 and Asp23 upon NQTrp binding. In contrast, our binding picture of Aβ1-28 monomer to NQTrp is fully consistent with the simulations of the Aβ1-42 dimer with two NQTrp [18], though the NQTrp contact probabilities change from Aβ1-28 to Aβ1-42 due to the absence of contacts between NQTrp and the residues Leu34 and Met35. This result, consistent with IE-MS experiments on the binding of small molecules to Aβ1-28 and Aβ1-42 peptides [21], adds support to the use of Aβ1-28 as a model for Aβ1-42.

Our results reveal that in the presence of NQTrp the populations of the 10 top visited clusters of the peptide increase from 67 to 72% using PCA analysis and the total number of clusters decreases by 26% using the RMSD metrics, in agreement with the previously computer-based observations that anti-amyloid inhibitors decrease the flexibility of short Aβ fragments [14]. Our simulations make it clear, however, that the presence of NQTrp is not sufficient to prevent the intrinsic disorder of the Aβ1-28 monomer.

In the presence of NQTrp, the population of β-hairpin is reduced by a factor of 1.5 and the population of α-helix in the region 17–24 is increased by a factor of two. These two factors, which impact the free energy barrier for nucleation, explain the lower Aβ1-40/1-42 aggregation kinetics in the presence of NQTrp. Another reason for the reported reduced aggregation kinetics results from the backbone and side-chain interactions of Aβ with NQTrp, making the peptide less prone to interact with another chain. The aromatic rings of NQTrp favor hydrophobic interactions with Aβ1-28, but they all have small lifetimes because of natural peptide flexibility.

NQTrp is found to enhance the α-helical structure probability of the residues 17–24 by a factor of two. Experimental studies on Aβ1-

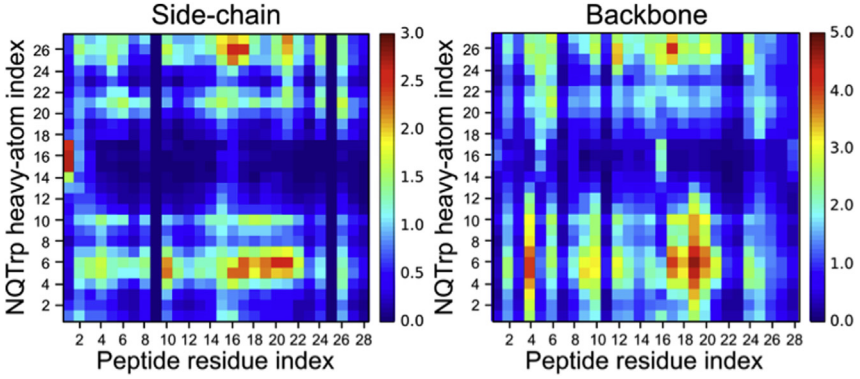

Fig. 8. Contact probabilities between the side-chain (left) and backbone (right) atoms of Aβ with the heavy atoms of NQTrp calculated over the time interval 50–205 ns at 315 K. The color code varies from 0 to 3% (left panel) and 0 to 5% (right panel).

40/Aβ1-42 have reported that the α-helix conformation is on-pathway to fibril formation [41–43] and the familial D7N mutation increases the aggregation kinetics by accelerating the transition from random coil to β-sheet [44]. Sequestering the residues Aβ17-24 in α-helical conformation for a longer time should slow down the transition to β-sheet, and in turn amyloid fibril formation. Our hypothesis is fully supported by the *in vitro* aggregation studies of Aβ1-28, Aβ1-28(Leu17Lys, Ala21Asp) variant and Aβ1-28 cyclo [Lys17–Asp21] with a lactam-bridge between the Lys17 and Asp21 side-chains. It was found that by bridging residues Lys17 and Asp21, the α-helix in this region was stabilized and could not unfold and the Aβ1-28 cyclo [Lys17–Asp21] could not form fibrils *in vitro*, while the un-bridged Aβ1-28(Leu17Lys, Ala21Asp) did [45].

Using extensive sampling with a force field able to fold many proteins to their native states [29] and a concentration of the peptide of 17.5 mM, we find that the fraction of free Aβ1-28 monomer in solution is on the order of 20–25%, indicating that NQTrp is a compound that can be improved to reduce the formation of dimer. Though this result is highly concentration dependent, Convertino et al. observed that NQTrp interacts 71% of the time with Aβ12-28 monomer in implicit solvent at a concentration of 2.5 mM and a molar ratio 1:1 of Aβ12-28: NQTrp [14]. Attasinasio et al. found, by using a total of 3 μs MD trajectory in implicit solvent at 300 K and a molar ratio of 1:1, that carnosine is in contact with Aβ1-42 monomer for only 20% of the time (and only 10% with Aβ1-28) at a concentration of 5 mM [11].

Our simulation results of the interaction between Aβ1-28 monomer and NQTrp at a molar ratio 1:1 and Aβ1-28 concentration set to 17.5 mM appear to be at odds with the SDS-PAGE and the Thioflavin-T binding essays which showed that inhibition is already apparent at a low 4–5:1 ratio of Aβ1-42:NQtrp with Aβ1-42 concentration set to 5 μM [13]. In contrast, our results are more consistent with ThT fluorescence of samples containing 100 μM Aβ1-42 incubated at 37 °C, and the 20% and 70% reductions in fluorescence using 5-fold and 20-fold molar excess of carnosine, respectively [11].

Overall our simulations show that the affinity of NQTrp is low and hence its inhibitory activity is not very strong. There is room to reduce the formation of dimer, a critical step in aggregation and toxicity [46]. We are further studying the anti-amyloid effect of NQTrp using atomistic REMD simulations of the dimer of Aβ1-28.

Contributors

B. Tarus and P.H. Nguyen performed the simulations and analyses. B. Tarus, O. Bertoumieu, P. Faller, A. Doig and P. Derreumaux wrote the manuscript. All authors have approved the final article.

Acknowledgments

This work was supported by grants from the “GRAL” ANR SIMI 12-BS07-0017-01 and Pierre Gilles de Gennes Foundation. We also acknowledge equipment support from “DYNAMO” ANR-11-LABX-0011.

References

[1] D.J. Selkoe, Folding proteins in fatal ways, Nature 426 (2003) 900–904.
[2] G.M. Shankar, S. Li, T.H. Mehta, A. Garcia-Munoz, N.E. Shepardson, I. Smith, F.M. Brett, M.A. Farrell, M.J. Rowan, C.A. Lemere, C.M. Regan, D.M. Walsh, B.L. Sabatini, D.J. Selkoe, Amyloid-beta protein dimers isolated directly from Alzheimer's brains impair synaptic plasticity and memory, Nat. Med. 14 (2008) 837–842.
[3] W.F. Xue, A.L. Hellewell, W.S. Gosal, S.W. Homans, E.W. Hewitt, S.E. Radford, Fibril fragmentation enhances amyloid cytotoxicity, J. Biol. Chem. 284 (2009) 34272–34282.
[4] M.G. Sharoar, M. Shahnawaz, M.I. Islam, V.S. Ramasamy, S.Y. Shin, I.S. Park, The inhibitory effects of Escherichia coli maltose binding protein on β-amyloid aggregation and cytotoxicity, Arch. Biochem. Biophys. 538 (2013) 41–48.
[5] T. Takahashi, H. Mihara, Peptide and protein mimetics inhibiting amyloid beta-peptide aggregation, Acc. Chem. Res. 41 (2008) 1309–1318.
[6] W. Hoyer, C. Grönwall, A. Jonsson, S. Ståhl, T. Härd, Stabilization of a beta-hairpin in monomeric Alzheimer's amyloid-beta peptide inhibits amyloid formation, Proc. Natl. Acad. Sci. U. S. A. 105 (2008) 5099–5104.
[7] R.D. Bell, M.D. Ehlers, Breaching the brain-blood barrier for drug delivery, Neuron 81 (2014) 1–3.
[8] H. Amijee, C. Bate, A. Williams, J. Virdee, R. Jeggo, D. Spanswick, D.I. Scopes, J.M. Treherne, S. Mazzitelli, R. Chawner, C.E. Eyers, A.J. Doig, The N-methylated peptide SEN304 powerfully inhibits Aβ(1-42) toxicity by perturbing oligomer formation, Biochemistry 51 (2012) 8338–8352.
[9] P. Pratim Bose, U. Chatterjee, C. Nerelius, T. Govender, T. Norström, A. Gogoll, A. Sandegren, E. Göthelid, J. Johansson, P.I. Arvidsson, Poly-N-methylated amyloid beta-peptide (Abeta) C-terminal fragments reduce Abeta toxicity in vitro and in Drosophila melanogaster, J. Med. Chem. 52 (2009) 8002–8009.
[10] J. Bieschke, M. Herbst, T. Wiglenda, R.P. Friedrich, A. Boeddrich, F. Schiele, D. Kleckers, J.M. Lopez del Amo, B.A. Grüning, Q. Wang, M.R. Schmidt, R. Lurz, R. Anwyl, S. Schnoegl, M. Fändrich, R.F. Frank, B. Reif, S. Günther, D.M. Walsh, E.E. Wanker, Small-molecule conversion of toxic oligomers to nontoxic β-sheet-rich amyloid fibrils, Nat. Chem. Biol. 8 (2011) 93–101.
[11] F. Attanasio, M. Convertino, A. Magno, A. Caflisch, A. Corazza, H. Haridas, G. Esposito, S. Cataldo, B. Pignataro, D. Milardi, E. Rizzarelli, Carnosine inhibits Aβ(42) aggregation by perturbing the H-bond network in and around the central hydrophobic cluster, Chembiochem 14 (2013) 583–592.
[12] L. Jiang, C. Liu, D. Leibly, M. Landau, M. Zhao, M.P. Hughes, D.S. Eisenberg, Structure-based discovery of fiber-binding compounds that reduce the cytotoxicity of amyloid beta, Elife 2 (2013) e00857.
[13] R. Scherzer-Attali, R. Pellarin, M. Convertino, A. Frydman-Marom, N. Egoz-Matia, S. Peled, M. Levy-Sakin, D.E. Shalev, A. Caflisch, E. Gazit, D. Segal, Complete phenotypic recovery of an Alzheimer's disease model by a quinone-tryptophan hybrid aggregation inhibitor, PLoS One 5 (2010) e11101.
[14] M. Convertino, A. Vitalis, A. Caflisch, Disordered binding of small molecules to Aβ(12-28), J. Biol. Chem. 286 (2011) 41578–41588.
[15] Y. Chebaro, P. Derreumaux, Targeting the early steps of Aβ(16-22) protofibril disassembly by n-methylated inhibitors: a numerical study, Proteins 75 (2009) 442–452.
[16] Y. Chebaro, S. Pasquali, P. Derreumaux, The coarse-grained OPEP force field for non-amyloid and amyloid proteins, J. Phys. Chem. B 116 (2012) 8741–8752; F. Sterpone, S. Melchionna, P. Tuffery, S. Pasquali, N. Mousseau, T. Cragnolini, Y. Chebaro, J.F. St-Pierre, M. Kalimeri, A. Barducci, Y. Laurin, A. Tek, M. Baaden, P.H. Nguyen, P. Derreumaux, The OPEP protein model: from single molecules, amyloid formation, crowding and hydrodynamics to DNA/RNA systems, Chem. Soc. Rev. 43 (2014) 4871–4893.
[17] Y. Chebaro, P. Jiang, T. Zang, Y. Mu, P.H. Nguyen, N. Mousseau, P. Derreumaux, Structures of Aβ17-42 trimers in isolation and with five small-molecule drugs using a hierarchical computational procedure, J. Phys. Chem. B 116 (2012) 8412–8422.
[18] T. Zhang, W. Xu, Y. Mu, P. Derreumaux, Atomic and dynamic insights into the beneficial effect of the 1,4-Naphthoquinon-2-yl-l-tryptophan inhibitor on Alzheimer's Aβ1-42 dimer in terms of aggregation and toxicity, ACS Chem. Neurosci. 5 (2014) 148–159.
[19] E. Mikros, D. Benaki, E. Humpfer, M. Spraul, S. Loukas, C.I. Stassinopoulou, M. Pelecanou, High-resolution NMR spectroscopy of the β-amyloid (1–28) fibril typical for Alzheimer's disease, Angew. Chem. Int. Ed. Engl. 40 (2001) 3603–3605.
[20] B.D. Moore, P. Chakrabarty, Y. Levites, T.L. Kukar, A.M. Baine, T. Moroni, T.B. Ladd, P. Das, D.W. Dickson, T.E. Golde, Overlapping profiles of Aβ peptides in the Alzheimer's disease and pathological aging brains, Alzheimers Res. Ther. 4 (2012) 18.
[21] E. Martineau, J.M. de Guzman, L. Rodionova, X. Kong, P.M. Mayer, A.M. Aman, Investigation of the noncovalent interactions between anti-amyloid agents and amyloid β peptides by ESI-MS, J. Am. Soc. Mass. Spectrom. 21 (2010) 1506–1514.
[22] B. Tarus, P.H. Phuong, P. Derreumaux, Familial Alzheimer A2V mutation reduces the intrinsic disorder and completely changes the free energy landscape of the Aβ1-28 monomer, J. Phys. Chem. B 118 (2014) 501–510.
[23] M. Coles, W. Bicknell, A.A. Watson, D.P. Fairlie, D.J. Craik, Solution structure of amyloid beta-peptide(1–40) in a water-micelle environment. Is the membrane-spanning domain where we think it is? Biochem. (Mosc.) 37 (1998) 11064–11077.
[24] H.J.C. Berendsen, D. van der Spoel, R. van Drunen, GROMACS: a message-passing parallel molecular dynamics implementation, Comput. Phys. Commun. 91 (1995) 43–56.
[25] J.-P. Ryckaert, G. Ciccotti, H.J.C. Berendsen, Numerical integration of the cartesian equations of motion of a system with constraints: molecular dynamics of n-alkanes, J. Comput. Phys. 3 (1997) 327–341.
[26] T. Darden, D. York, L. Pedersen, Particle mesh Ewald: an N log(N) method for Ewald sums in large systems, J. Chem. Phys. 98 (1993) 10089–10092.
[27] G. Bussi, D. Donadio, M. Parrinello, Canonical sampling through velocity rescaling, J. Chem. Phys. 126 (2007) 014101.
[28] P.H. Nguyen, M.S. Li, P. Derreumaux, Effects of all-atom force fields on amyloid oligomerization: replica exchange molecular dynamics simulations of the Aβ(16–22) dimer and trimer, Phys. Chem. Chem. Phys. 13 (2011) 9778–9788.

[29] K. Lindorff-Larsen, S. Piana, R.O. Dror, D.E. Shaw, How fast-folding proteins fold, Science 334 (2011) 517–520.
[30] P. Derreumaux, M. Dauchez, G. Vergoten, The structures and vibrational frequencies of a series of alkanes using the SPASIBA force field, J. Mol. Struct. 295 (1993) 203–221.
[31] P. Derreumaux, G. Vergoten, P. Lagant, A vibrational molecular force field of model compounds with biological interest. I. Harmonic dynamics of crystalline urea at 123 K, J. Comput. Chem. 11 (1990) 560–568.
[32] Marvin Version 5.12.2, ChemAxon, 2013. http://www.chemaxon.com.
[33] Suite 2012: Maestro, Version 9.3, Schrödinger, LLC, New York, NY, 2012.
[34] ParamChem interface: https://www.paramchem.org.
[35] K. Vanommeslaeghe, E.P. Raman, A.D. MacKerell Jr., Automation of the CHARMM General Force Field (CGenFF) II: assignment of bonded parameters and partial atomic charges, J. Chem. Inf. Model 52 (2012) 3155–3168.
[36] K. Vanommeslaeghe, E. Hatcher, C. Acharya, S. Kundu, S. Zhong, J. Shim, E. Darian, O. Guvench, P. Lopes, I. Vorobyov, A.D. Mackerell Jr., CHARMM general force field: a force field for drug-like molecules compatible with the CHARMM all-atom additive biological force fields, J. Comput. Chem. 31 (2010) 671–690.
[37] A. Patriksson, D. van der Spoel, A temperature predictor for parallel tempering simulations, Phys. Chem. Chem. Phys. 10 (2008) 2073–2077.
[38] D. Frishman, P. Argos, Knowledge-based protein secondary structure assignment, Proteins 23 (1995) 566–579.
[39] M.H. Viet, P.H. Nguyen, S.T. Ngo, M.S. Li, P. Derreumaux, Effect of the Tottori familial disease mutation (D7N) on the monomers and dimers of Aβ40 and Aβ42, ACS Chem. Neurosci. 4 (2013) 1446–1457.
[40] R. Scherzer-Attali, M. Convertino, R. Pellarin, E. Gazit, D. Segal, A. Caflisch, Methylations of tryptophan-modified naphthoquinone affect its inhibitory potential toward Aβ aggregation, J. Phys. Chem. B 117 (2013) 1780–1789.
[41] C. Soto, N.C. Inestrosa, The alpha-helical to beta-strand transition in the amino-terminal fragment of the amyloid beta-peptide modulates amyloid formation, J. Biol. Chem. 270 (1995) 3063–3067.
[42] Y. Takahashi, T. Yamashita, A. Ueno, H. Mihara, Construction of peptides that undergo structural transition from α-helix to β-sheet and amyloid fibril formation by the introduction of N-terminal hydrophobic amino acids, Tetrahedron 56 (2000) 7011–7018.
[43] M.D. Kirkitadze, M.M. Condron, D.B. Teplow, Identification and characterization of key kinetic intermediates in amyloid beta-protein fibrillogenesis, J. Mol. Biol. 312 (2001) 1103–1119.
[44] K. Ono, M.M. Condron, D.P. Teplow, Effects of the English (H6R) and Tottori (D7N) familial Alzheimer disease mutations on amyloid beta-protein assembly and toxicity, J. Biol. Chem. 285 (2010) 23186–23197.
[45] A. Kapurniotu, A. Buck, M. Weber, A. Schmauder, T. Hirsch, J. Bernhagen, M. Tatarek-Nossol, Conformational restriction via cyclization in beta-amyloid peptide Abeta(1–28) leads to an inhibitor of Abeta(1–28) amyloidogenesis and cytotoxicity, Chem. Biol. 10 (2003) 149–159.
[46] P.H. Nguyen, P. Derreumaux, Understanding amyloid fibril nucleation and Aβ oligomer/drug interactions from computer simulations, Acc. Chem. Res. 47 (2014) 603–611.